

# AUTONOMY IN GUIDANCE USING IMAGE-BASED TERRAIN RECOGNITION AND OPTICAL NAVIGATION

Toshihiko Misu  
Tatsuaki Hashimoto  
Keiken Ninomiya

The Institute of Space and Astronautical Science  
3-1-1, Yoshinodai, Sagami-hara, Kanagawa 229-8510, Japan  
misu@nsl.isas.ac.jp

## Abstract

In this paper, we propose a scheme of autonomous guidance of spacecraft based on grayscale image. The autonomous guidance consists of 2 key technologies; topographic recognition and optical navigation. First, the pixel brightness in an image of the target surface is directly evaluated (without shape reconstruction) using a look-up table. A fuzzy-like logic determines an appropriate target site for landing, scientific observation, etc. Then, the spacecraft autonomously navigates itself by fixating visually characteristic areas in the surface image. The on-off thruster control is used to guide the spacecraft to the target site. By repeating the target designation and the optical navigation, we can guide the spacecraft to various interesting sites safely. Computer simulations showed its validity and capability for practical applications.

**Key words:** Autonomy, Topographical Recognition, Optical Navigation, Guidance.

## Introduction

Recently, a number of exploration programs to the bodies in deep space are planned and some of them are executed. There are various kinds of strategies to explore such bodies: fly-by, orbiter, rover, etc. Now, more sophisticated strategy, such as sample-and-return, is assumed to be one of the most powerful ones that enables precise investigation on the origin of the solar system, and is the focus of scientists' interest. Moreover, the target ranges from large planet to small satellite and even mysterious small bodies such as comet and asteroid.

To accomplish such complex missions to bodies of which details are not known, it is important to have the spacecraft possess a kind of autonomy in its navigation, guidance and control. Long round-trip delay and narrow bandwidth of the communication between the spacecraft and the Earth limit the scopes of real-time maneuvers in obstacle avoidance and location hunting for

scientifically interesting sites on the terrain. So, environment recognition and autonomous positioning would play important roles in deep-space missions in the future.

On the other hand, small spacecraft are supposed to be a solution that enables us to keep appropriate frequency and efficiency of exploration within a limited budget. For such spacecraft (and not limited to small ones), it is essential to use small, light, and good instruments both in science observation and navigation. Development of imaging instruments such as CCD cameras is so radical and wonderful that we can take high-resolution (millions of pixels) images with a palmtop camera of fairly low price. In this paper, we propose a method for the autonomous guidance of spacecraft in the vicinity (tens of kilometers to tens of meters away) of the target celestial body using grayscale camera images.

The guidance scheme mainly consists of two technologies. One of them is fast autonomous terrain recognition from a grayscale image, which designates a favorable site on the surface of the body. Demands are expressed in several basal topographic categories, logic operations, modifier, image scaling, and positional arrangement. Demands such as "look for a very flat plane near to a large mountain with a small crater" can be expressed. Then, the spacecraft autonomously extract some visually characteristic features (fixation point) from an image taken by the onboard camera. Tracking the fixation point, the spacecraft can estimate the movement of itself. Controlling thruster operations, the spacecraft approaches to the target site designated by the topographic recognition. As a result, the combination of these two technologies realizes a stable and intelligent guidance that can recognize and explore unknown feature of the terrain.

## Autonomous Optical Navigation

In this section, we describe an autonomous optical navigation method<sup>1</sup> used in the autonomous guidance, which guides the spacecraft to a landing/observation site designated by a topographic recognizer.

To guide the spacecraft to a (landing) site, if the site itself has visually characteristic features that are easily identified in the acquired images, the guidance would be so easy; only visually fixate the site and just approach it. But, if no distinct feature is visible at the site, the guidance may fail.

### Extraction of Fixation Points

To overcome the problem of tracking failure, some visually characteristic areas (fixation points; FP's) are automatically extracted from an image taken by a navigation camera to be used for visual tracking which determines relative position between the target point and the spacecraft. The fixation points are not needed to be identical to the target point. So, the spacecraft can be guided to any target site even if the target (e.g., very flat plane) itself has no distinct visible features in the image. This is the very essence of our optical navigation.

In the FP tracking, we employed the block-matching algorithm that minimizes the total square error of local region between the images. In order to strengthen the robustness of FP's in the visual tracking, following two conditions are needed:

1. *The spatial wavelength of gradation of intensity should be comparable to the size of matching template.*
2. *High contrast feature should be observed.*

To implement the first item, the image (of the target surface) is spatially band-pass-filtered. The filter consists of sub-sampling with smoothing (averaging), and Laplacian filtering.

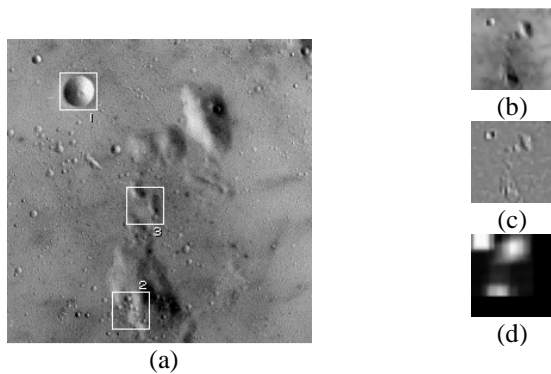


Figure 1: Result of extraction of fixation points

Fig. 1 shows an example of FP extraction. First, an original image (a) is blurred and sub-sampled to be (b). We can see that small features are omitted. And, Laplacian filter filters high-frequency information as shown in (c). Then, local variance of the image (c) is

calculated. Brighter region in (d) means high variance. The boxes in (a) are extracted FP's from high-variance areas of (d). Visually characteristic areas with features of comparable wavelength to the white boxes in the image are extracted.

### Overview of the Optical Navigation

By tracking FP('s), the spacecraft (S/C) can estimate the movement of itself relative to the target surface.

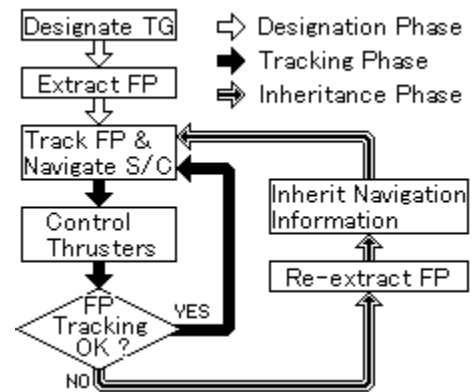


Figure 2: Navigation based on FP tracking

Fig. 2 is the flowchart of our optical navigation. First, the target point is designated, and S/C automatically extract visually characteristic area as FP. Onboard computer on S/C tracks the FP using block-matching algorithm to estimate relative position between TG and S/C. In case of failure of FP tracking at the next imaging loss expected, a new FP is re-extracted in order not to lose TG. Otherwise, tracking of the same FP is continued.

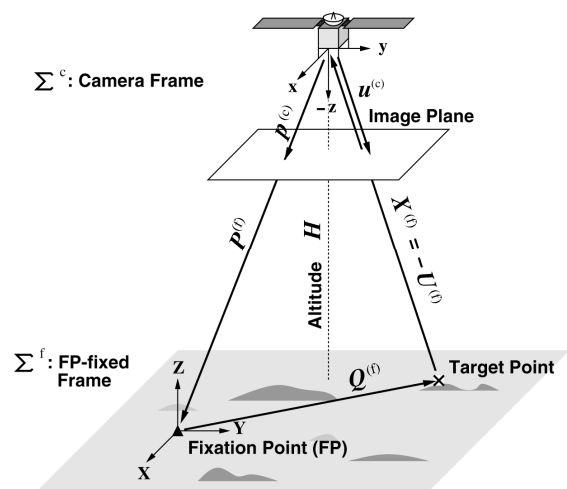


Figure 3: Geometry

The flow of the navigation is divided into 3 phases: *Target Designation Phase*, *Tracking Phase*, and *Fixation-Point Inheritance Phase*.

### Target Designation Phase

First, a target point (TG) on/above the celestial body is designated. The spacecraft shall be guided to the target point. As shown in Fig. 3, the position  $\vec{u}^{(c)}$  of TG in the image is converted to the vector  $\vec{X}^{(f)}$  from TG to S/C using altitude  $H$  and attitude information. In this paper, we assume that the attitude of S/C is controlled to have the camera frame be parallel to the FP-fixed coordinate system for simplicity.

If the TG is lying on the surface of the body,

$$\vec{X}^{(f)}(0) = -\frac{H(0)}{f}\vec{u}^{(c)}(0),$$

where  $f$  is the focal length of the navigation camera. Similarly, FP on the image is also converted to a three-dimensional vector  $\vec{P}^{(f)}$  in the FP-fixed frame:

$$\vec{P}^{(f)}(0) = \frac{H(0)}{f}\vec{p}^{(c)}(0).$$

Then, the vector  $\vec{Q}^{(f)}$  from FP to TG is calculated as follows:

$$\vec{Q}^{(f)}(0) = \vec{P}^{(f)}(0) + \vec{X}^{(f)}(0).$$

### Tracking Phase

The vector  $\vec{Q}^{(f)}(0)$  is used to get the S/C position relative to TG from the result of FP-tracking as follows:

$$\begin{aligned}\vec{P}^{(f)}(t) &= \frac{H(t)}{f}\vec{p}^{(c)}(t) \\ \vec{X}^{(f)}(t) &= \vec{Q}^{(f)}(0) - \vec{P}^{(f)}(t).\end{aligned}$$

### Fixation-Point Inheritance Phase

As the S/C approaches to TG, FP would become unsuitable for tracking, because the FP moves on the image plane to go out the field of view of the camera. If

such situation is detected, a new FP is re-extracted to change object of the fixation.

### Topographic Recognition

In this section, we propose a topographic recognition method that designates an appropriate site for landing, observation, etc. Qualitative recognition (e.g., “a small mountain in a large crater”) is performed without quantitative shape reconstruction (e.g., stereo vision, shape from shading algorithm, etc.) from a monocular grayscale image.

Fig. 4 depicts the structure of the recognizer. An observed grayscale image and several topographic categories (e.g., “mountain,” “concavity,” etc.) are compared using a look-up-table which relates the brightness of a pixel with the direction of normal vector of the target surface. The result of the comparison is expressed in a kind of fuzzy truth value. The truth values for some topographic categories are input to a logic expression in order to extract suitable area(s) for scientific/technological demands.

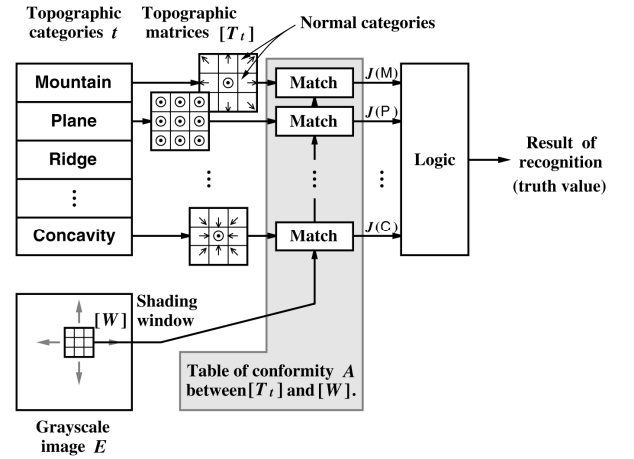


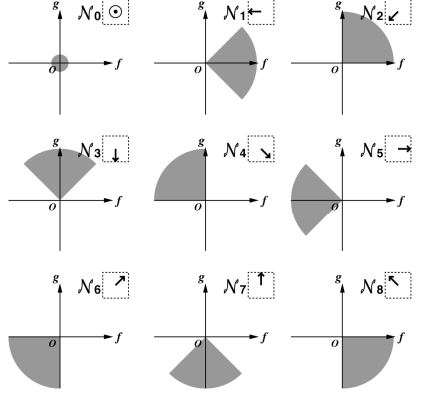
Figure 4: Structure of topographic recognition

### Normal Categories

We use  $(x, y, z)$  to point a place in the the 3-dimensional space ( $z$  is for the altitude). In this paper, we assume that the projection of camera is orthographic one, for simplicity. So,  $(x, y)$  are the image coordinates as well.

In order to express topographic categories in the recognition, we use several categories (normal categories) of normal direction. Each normal category is a subspace of gradient space as shown in Fig. 5, where  $(f, g) = (\partial z/\partial x, \partial z/\partial y)$ . In this case, there are 9

categories: (0) upward, (1) west, (2) southwest, (3) south, (4) southeast, (5) east, (6) northeast, (7) north, and (8) northwest.



The arrows in the boxes  $\square$  are top views of the normal vectors.

**Figure 5: Normal categories**

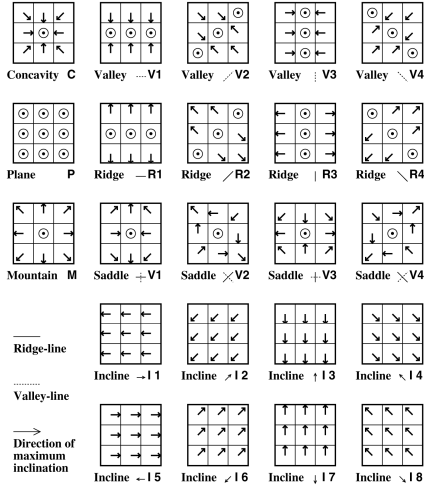


**Figure 6: Topographic categories**

### Topographic Categories

Piling 9 normal categories into a  $3 \times 3$ -matrix, we can define qualitative topographic features as shown in Fig. 6. We defined 7 main topographic categories: mountain, ridge, plane, valley, concavity, saddle, and incline in the recognition. And, ridge, valley, saddle, and incline are subcategorized into eight (for “incline”) or four (for other categories) subcategories with respect to their direction of slope or ridge/valley line.

### Look-Up-Table

Here, we show how to make a look-up-table (LUT) which gives the index of “conformity” with respect to the observed brightness of the pixel and each normal category. First, it is necessary to assume a type of reflectance of the target surface. If the surface is Lambertian, for example, the reflectance  $R(f, g)$  with respect to the gradient  $(f, g)$  of target surface is expressed as follows:

$$R(f, g) = \max \left\{ \frac{\vec{l} \cdot [f, g, -1]^T}{\sqrt{f^2 + g^2 + 1}}, 0 \right\},$$

where  $\vec{l}$  is a direction vector of the incident light. The “equi-reflectance map” is defined as follows:

$$\Gamma(E; f, g) = \gamma(f, g) \cdot e^{-\lambda \{R(f, g) - E\}^2},$$

where  $E$  is the observed brightness of a pixel, and  $\gamma(f, g)$  is a kind of weighting function. Then, we define the LUT  $A(E, n)$  as follows:

$$A(E, n) = \frac{\iint_{N_n} \Gamma(E; f, g) df dg}{\iint_{N_n} 1 df dg},$$

where  $N_n$  is a gradient sub-space shown in Fig. 5.

### Topographic Scale

It is important to consider the “scales” of features in a topographic description.

As depicted in Fig. 7, the “scale” of topographic features is reflected to the recognition by the operations of smoothing (a)  $\rightarrow$  (b) and sampling (c)  $\rightarrow$  (d). The larger feature is recognized by the larger  $s$ . In this method, the “scale” is measured on the image plane. Thus, projection from real length to pixels using altitude information would be necessary if the scale in real space is needed.

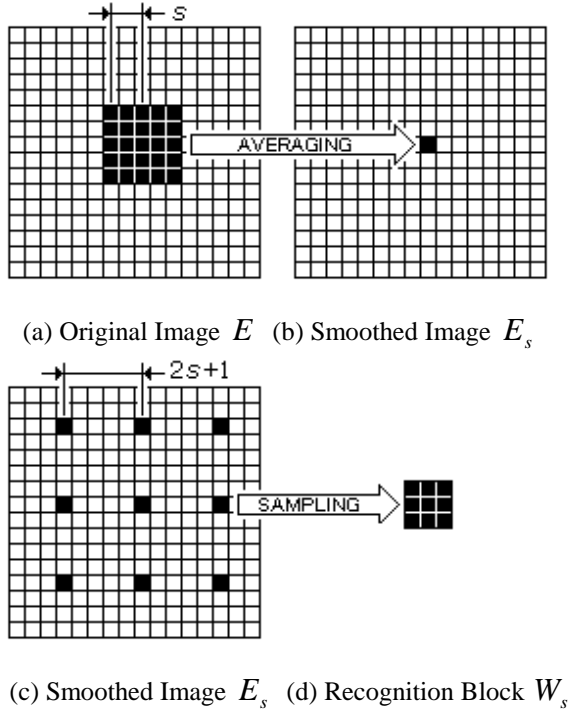


**Figure 7: Recognition block**

### Calculation of Truth Value

The truth values  $J(t; W)$  is calculated by making product of  $A(E, n)$  for all 9 pixels of the recognition block:

$$\tilde{J}(t; W) = \kappa(t) \prod_{j=-1}^1 \prod_{i=-1}^1 A(W(i, j), T_{t, i, j})$$

$$J(t; W) = \tilde{J}(t; W) / \sum_{\tau} \tilde{J}(\tau; W),$$

where  $T_t$  is a topographic template (see Fig. 6) which consists of 9 normal categories (the  $n$ 's of  $N_n$ 's) for a specified topographic category  $t$ , and  $\kappa(t)$  is a weighting coefficients.

### Logic Operations

We introduce 3 logic operations:

AND:  $J_1 \wedge J_2 = \min(J_1, J_2)$

OR:  $J_1 \vee J_2 = \max(J_1, J_2)$

NOT:  $\neg J = 1 - J$ ,

and linguistic modifier  $M(m, J) = J^m$ , where larger  $m (> 0)$  results in a “severe” evaluation.

### Example of Topographic Feature Extraction

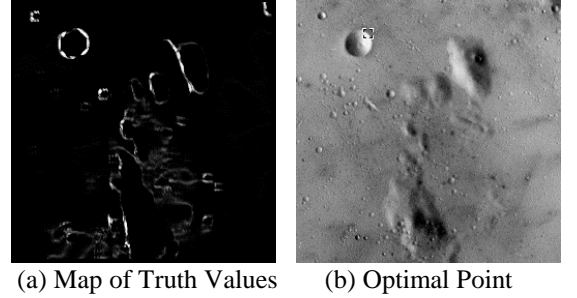


**Figure 8: Extraction of crater rim**

By substituting the truth values for all/some topographic categories to logic expressions (with modifiers, if necessary), we can designate various features:

1. Mountain in the scale 1:  $J(M; W_1)$
2. Mountain or plane:  $J(M; W_1) \vee J(P; W_1)$
3. Very flat plane:  $M(2, J(P; W_1))$ ,

where  $M$  and  $P$  means “mountain” and “plane,” respectively (abbreviations for other topographic categories are shown in Fig. 6). In this paper, we use abbreviated form  $X_s^m = M(m, J(X; W_s))$  which means “topographic category  $X$  of scale  $s$  with linguistic modification  $m$ .” The cases listed above become  $M_1^1$ ,  $M_1^1 \vee P_1^1$ , and  $P_1^2$ , respectively.

Substituting  $J(t; W)$ 's to the logic expression, we can extract appropriate sites which meet the expression. To extract crater rim, for example, the logic would be  $R_1^1 \vee R_2^1 \vee R_3^1 \vee R_4^1$ . The result of the extraction is shown in Fig. 8. Fig. 8(a) is the distribution map of truth values. And, the point with the greatest truth value is pointed by a small square in (b). A site on the north-east side of a crater rim is extracted.

### Autonomous Guidance

The combination of the optical navigation and the topographic recognition realizes an autonomous guidance system. As shown in Fig. 9, a target site for landing/observation is designated by the topographic recognition based on topographic demands written in logic expressions. Then the thrusters of the S/C are

controlled to guide S/C to the site using information on relative position by the optical navigation. In this section, a simulation on autonomous guidance is shown.

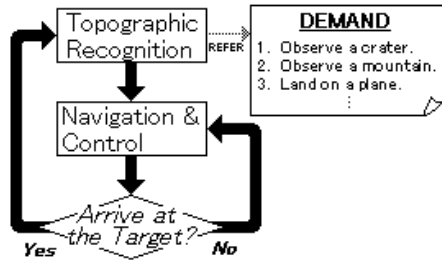


Figure 9: Flowchart of the autonomous guidance

### Simulation

Table 1: Topographic demands in a mission

TG No.	Time [s]	Altitude [m]	Topographic Demand	Logic Expression
	0	400	<i>Initial Position</i>	
TG <sub>1</sub>	330	300	Ridge	$R1_1 \vee R2_2 \vee R3_3 \vee R4_4$
TG <sub>2</sub>	660	250	Small Crater	$C_1$
TG <sub>3</sub>	990	250	Large Crater	$C_3$
TG <sub>4</sub>	1320	250	Huge Crater	$C_6$
TG <sub>5</sub>	1550	200	Plane	$P_1 \wedge P_2 \wedge P_3$

Table 1 describes an example of the exploration plan. Initially, in this case, the S/C is hovering above the target terrain at the altitude of 400 [m]. The first target is a small ridge in the image taken from the initial position.

Using the logic expression in the table, a target point TG<sub>1</sub> on the crater rim is selected as shown by white cross in Fig. 10(a). And simultaneously, an FP is also extracted (the square in Fig. 10(a)) to be visually tracked in (b), (c) and (d). But, in Fig. 10(d), as the FP translates too lower to continue tracking, another FP is extracted (the square at the top-right corner of (d)) to inherit the navigation information. The new FP is tracked after the frame (e). Finally, the S/C arrived at the altitude of 300 [m] above the TG<sub>1</sub> (Fig. 10(f)). Then, the second target TG<sub>2</sub> (a “small crater”) is autonomously extracted as shown in (g), and the S/C reached it at the frame (h). The departure and arrival of the S/C with the 3rd demand “large crater” are shown in Fig. 10(i), (j).

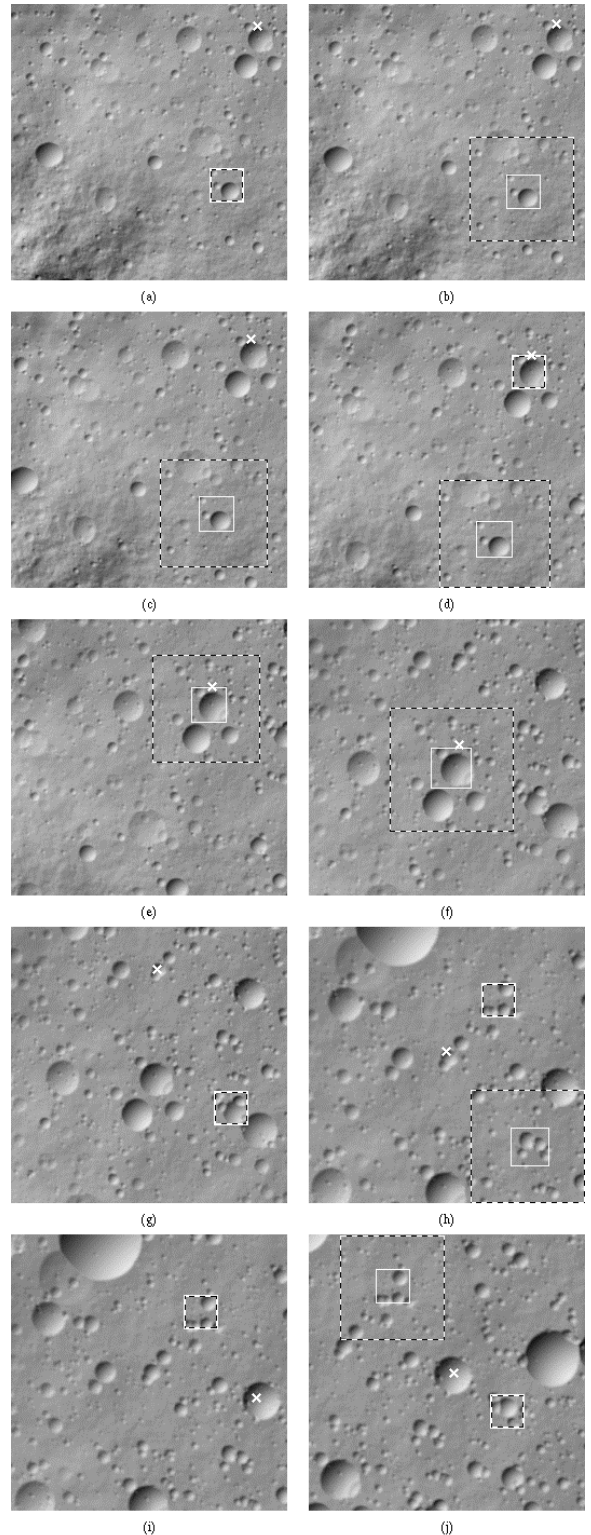
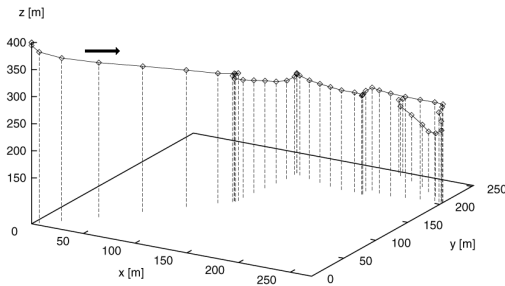
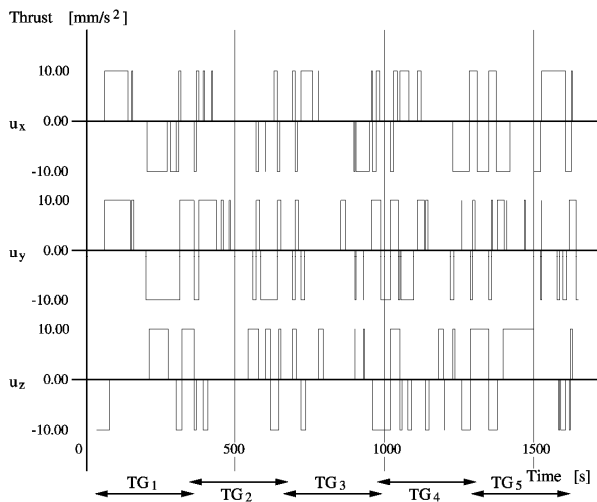


Figure 10: Simulated images taken by the spacecraft

The trajectory of the S/C through the whole sequence (from the initial position to the TG<sub>5</sub>) is plotted in Fig. 11. We can see that the S/C explores those 5 targets sequentially.



**Figure 11: Trajectory of the spacecraft**



**Figure 12: On-off control pattern of the thrusters**

The pulses shown in Fig. 12 are acceleration and deceleration maneuvers for each pair of thrusters (the thrusters are aligned parallel to the 3 orthogonal axes of the S/C). The pattern mainly consists of 5 sets of three states; acceleration, coasting, and deceleration with narrow pulses which correct the guidance error caused by the tracking and ranging errors.

## Conclusion

In this paper, following technologies are proposed:

1. optical navigation based on fixation-point tracking,
2. topographic recognition based on a grayscale image, and
3. autonomous guidance system as a fusion of the items 1 and 2.

The guidance scheme enables the spacecraft explore almost unknown celestial body safely. Moreover, demands from scientific interests can also be considered in the target selection.

## Acknowledgment

This research is enabled by the courtesy of Grant-in-Aid for JSPS fellows (Subject No. 8-04758) by Ministry of Education, Science and Culture of Government of Japan.

## Reference

- <sup>1</sup>Misu, T; Hashimoto, T; Ninomiya, K. Optical Guidance for Autonomous Landing of Spacecraft, *IEEE Transactions on Aerospace and Electronic Systems*, Vol. 35, No. 3, July 1999 (to appear).